

A low-frequency, high-amplitude, torsional oscillator for studies of quantum fluids and solids

Anthony M. Guénault,^{1, a)} Peter V. E. McClintock,¹ Malcolm Poole,^{1, b)} Roch Schanen,¹ Viktor Tsepelin,¹ Dmitry E. Zmeev,¹ David Schmoranzner,² William F. (“Joe”) Vinen,^{3, c)} Deepak Garg,⁴ and Kalpana Devi⁴

¹⁾*Department of Physics, Lancaster University, Lancaster LA1 4YB, United Kingdom*

²⁾*Faculty of Mathematics and Physics, Charles University, Prague, Czech Republic*

³⁾*School of Physics and Astronomy, University of Birmingham, B15 2TT, United Kingdom*

⁴⁾*D.A.V. College affiliated to Panjab University, Chandigarh-160011, India*

(Dated: 5 April 2023)

We introduce a low-frequency torsional oscillator suitable for studies of quantum fluids and solids. It operates at frequencies of ~ 100 Hz, achieves velocities of several cm s^{-1} , and exhibits a quality factor of $Q \simeq 3 \times 10^4$. In order to reach such velocities at this relatively low frequency, the oscillator amplitude must exceed $100 \mu\text{m}$, which would be impracticable for a conventional capacitor-driven device where the drive is applied parallel to the main motion and there are correspondingly large changes in the separation of the capacitor plates. For the different geometry of the oscillator that we now describe, however, the separations of both the drive and detect capacitor plates remain constant regardless of the amplitude of oscillation. We discuss its design, and report our initial tests of its performance.

Torsional oscillators have been a valuable tool in studies of quantum fluids and solids since the very beginning. For example, they have been used to detect phase transitions in liquid ^4He ¹ and helium isotopic mixtures², in 2D adsorbed helium films and in restricted geometries^{3,4} and porous media^{5–8}.

The most direct experiment searching for the supersolid phase in bulk solid ^4He also used the torsional oscillator technique⁹: the onset of superfluidity in the solid helium inside a torsional oscillator would have decreased the overall moment of inertia, and hence decreased the resonant period. Bishop et al. made measurements of solid helium from 25 to 48 bar, and concluded that, if there was a supersolid state, then either the supersolid fraction (the fraction of ^4He atoms participating in superflow) was less than 5×10^{-6} or the critical velocity (maximum velocity of superflow without any detectable dissipation) was less than $5 \mu\text{m s}^{-1}$ ⁹. Kim and Chan^{10,11} employed this same technique for the detection of an anomalous response in solid helium. Others soon followed with a variety of designs and experiments. These included compound torsional oscillators to study the frequency dependence of the nonclassical rotational inertia of solid ^4He ^{12,13}, a torsional oscillator in conjunction with a square cell¹⁴ for similar studies, a cell capable of measuring the torsional oscillation and shear modulus simultaneously using a piezo-transducer, under uniform rotation¹⁵ and, more recently, a compound torsional oscillator to show the existence of a 2D spatially-modulated superfluid¹⁶. In common to all of these designs was the use of capacitive drive and detect systems. For a conventional torsional oscillator, Seamus Davis’s group introduced a magnetic pick up using a SQUID¹⁷, making it sensitive to much smaller displacements and velocities.

Our immediate motivation for developing the present oscillator is to study quantum turbulence (QT). It is the most general form of dissipative motion in superfluids, and it differs

from its classical counterpart mainly by the inherent quantization of fluid circulation, which manifests itself as the existence of *quantized vortices*^{18,19}. These vortices are identical to each other in all respects save position and core velocity. They not only serve as the building blocks for macroscopic quantum flows, but they also provide the only means of energy dissipation in a pure superfluid that has zero viscosity²⁰. It is presently understood that Kelvin wave excitations on these vortices transfer energy to progressively shorter wavelengths, until it is radiated as excess thermal quasiparticles in $^3\text{He-B}$ or as sound excitations in ^4He and Bose-Einstein condensates (BECs). In the case of superfluid ^4He , the onset of QT is characterised by the critical velocity needed for self-reconnection of the Kelvin waves on remanent vortices²¹ attached to walls and surfaces.

At temperatures above $\sim 0.7\text{K}$, vortex dynamics in ^4He becomes complicated because of a significant density of viscous normal fluid component (quasiparticles). This requires the use of phenomenological e.g. HVBK^{22,23} or geometrical^{24–26} models to describe the QT and its decay²⁷ when the thermal or mechanical driving force is removed. Our interest, however, centres on the simpler situation that pertains in the low temperature limit where the effect of normal fluid can be ignored. Even then, when only the superfluid component need be considered, there still remains much to be understood, and fascinating new ideas are being introduced on a regular basis, e.g. the recent identification of “fine structure” in the energy levels of model vortex rings in a cylindrical domain.²⁸

Our main concern here is to develop the technology needed to study QT creation through the excitation of Kelvin waves. To generate waves of sufficient amplitude for reconnection to occur requires that we lower the frequency range of operation, compared to most earlier oscillators and, at the same time, that we increase the velocity range. These are seemingly opposed ambitions because a reduction in frequency at a given amplitude must also reduce the velocity. We report here a design that allows us to fulfill our goal but, in order to appreciate its unusual mode of operation, we first summarise the design and function of a traditional cryogenic oscillator.

^{a)}Deceased October 30, 2019

^{b)}Corresponding Author e-mail m.poole@lancaster.ac.uk

^{c)}Deceased June 8, 2022

A common design is illustrated in Figs. 1(a) and (b). The oscillator, shown in yellow in (b), is composed of a cylindrical body and a support rod. The body contributes to the total moment of inertia I and the support rod provides the necessary return spring, with spring constant k . To drive the oscillator and measure its motion, two capacitors are used. Each of them is formed of a moving electrode (shown in blue) attached to the main body, and a fixed electrode (red). Each pair of electrodes is separated by a very small gap on the order of $100\ \mu\text{m}$.

The capacitors are each charged to a substantial DC voltage, so that the plates strongly attract. An additional AC potential is then applied to the driving capacitor, which causes small oscillations of the moving plate and thus of the oscillator body to which it is fixed. The corresponding capacitance changes in the second transducer induce a small AC current to its fixed electrode, measured by a phase-sensitive detector referenced to the AC drive. This system works well at small amplitudes, but is constrained by the very narrow plate separations needed in the capacitors.

To investigate the onset of QT creation, we wish to study the oscillation of a pill-box-shaped experimental cell as sketched in Fig. 2. At low temperatures, in the absence of vortices, the coin-shaped sample of superfluid within the cell would remain stationary within the oscillating structure. However, it is to be expected that, prior to oscillation, there will exist remanent vortices²¹ pinned between the top and bottom plates, parallel to the axis of symmetry. The movements of the oscillator will induce Kelvin waves on these vortices and, for sufficient wave amplitude, there will be vortex reconnections, production of QT, and significant dissipation. For typical vortices of length between several hundreds of micrometers up to millimeters, the Kelvin wave resonant frequencies are hundreds of Hz. The critical velocity, v_c , is proportional to the square root of the angular frequency ω , and we need to bring v_c down into the measurable range. Based on dynamics of quantized vortices, the critical velocity for inducing reconnections can be estimated²⁹ as $v_c \approx \sqrt{8\kappa\omega}$, where $\kappa = 9.97 \times 10^{-8}\ \text{m}^2\text{s}^{-1}$ is the quantum of circulation in ^4He . It is estimated that $Q > 10^4$ will be sufficient to detect the dissipation corresponding to the onset of reconnections at this critical velocity.

Thus for frequencies near 100 Hz, critical velocities of order $20\ \text{mm s}^{-1}$ are expected, corresponding to amplitudes near $30\ \mu\text{m}$ at the circumference of the superfluid-filled cell. To search for convincing evidence of QT production, the critical velocity must be exceeded substantially, which is impossible using the conventional oscillator design because the capacitor plates would be liable to touch, given the large oscillation amplitude required. To solve this problem we use a transducer geometry that moves the electrodes *parallel* to the motion of the torsional oscillator, so that they cannot touch even at the largest amplitudes and corresponding velocities. The oscillator drive and detection capacitors have partially overlapping electrodes. Electrostatic shear forces are therefore generated in the plane of the capacitor plates; and the capacitance changes with the area of overlap, leaving the small distance between the plates unaffected. We use the same external electrical drive and detection systems as for the conventional oscillator³⁰. As we demonstrate below, this kind of oscillator

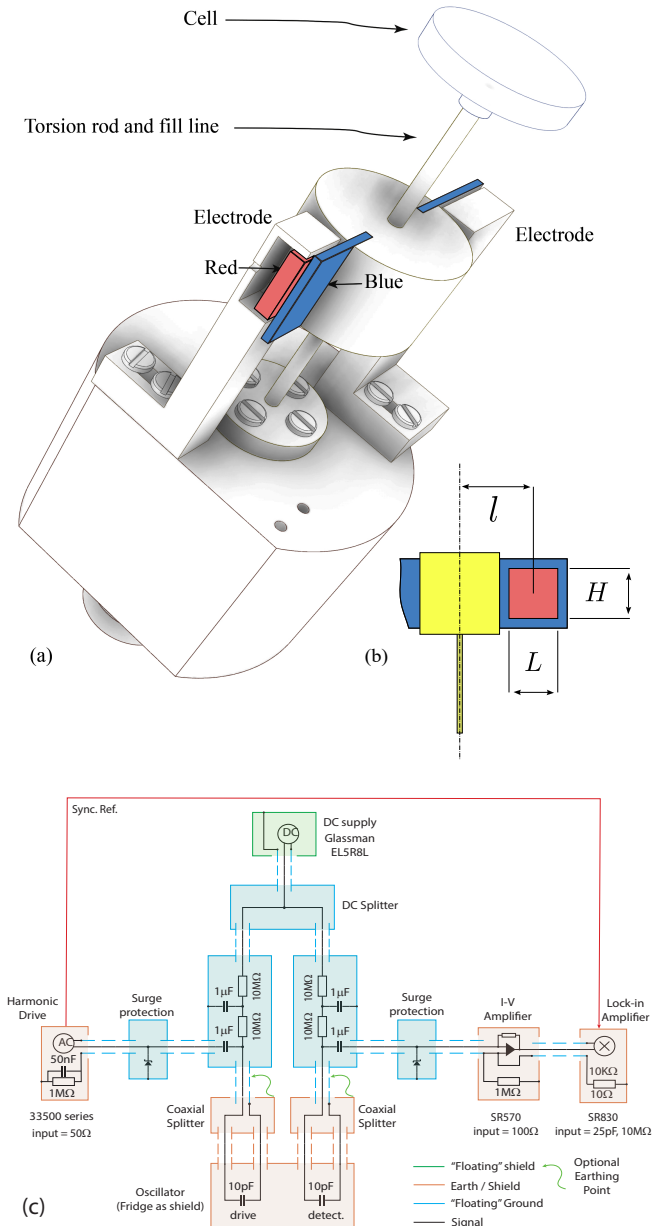


FIG. 1. (a). Common design for a cryogenic torsional oscillator. (b) Side view showing the main body of the oscillator, the torsion rod, the positions l and size $L \times H$ of each fixed plate. (c) Schematic electrical circuit used for running the torsional oscillator showing all instruments used in the experiment. Also shown are the protection diodes and capacitors with the wiring and grounding in the circuit. The gain setting of the SR570 Amplifier is $1\ \mu\text{A/V}$.

can achieve velocities of up to at least $300\ \text{mm s}^{-1}$, giving stable and reproducible vacuum data. Its design and construction are shown in Fig. 2. As in a conventional torsional oscillator, the active elements are parallel plate capacitors charged to a high DC bias voltage, and with an AC voltage superimposed in the case of the driving electrodes. The shear forces due to the incomplete overlap of the capacitor plates tend to increase

the overlap and to bring the plates towards alignment.

To make full use of this effect, and to spread the force evenly around the torsional oscillator, we developed the design illustrated in Fig. 2 (a). For our particular experiments, a sample of liquid ^4He is located in a pill-box-shaped epoxy cell fixed to the centre of a rigid copper framework by a BeCu tube, which forms the torsion rod. This tube is attached rigidly to the top and bottom of the framework, and has a small hole in its side at the centre so that it also acts as the fill line for the cell. This highly symmetrical design helps to ensure that the oscillator does not respond to unwanted nuisance modes at nearby frequencies. Each electrode consists of 12 evenly-spaced sectors, electrically connected together, manufactured using conventional lithographic techniques on a thin circular circuit board of radius 2 cm. The radial segments between radii r and R are distributed in a star-like fashion and connected by a small ring. Two finned electrodes of the type described above are permanently fixed to the top and bottom of the cell. Very close to them, two similar finned electrodes are positioned above and below, with deliberate angular misalignments of one half-segment-width, as illustrated in Figs. 2 (b) and (c). They are attached to the frame and carefully adjusted to create a narrow gap d for each capacitor, one of which is used to drive the oscillator and the other to detect its motion.

To analyse the physics of the oscillator, we first consider an idealised system, where the capacitance between the individual pairs of electrode segments is taken as that of a parallel-plate capacitor. Thus we neglect, *inter alia*, stray capacitances to ground and to the copper support rods/rings, and the effects of the finite conductivity of the circuit board material (but see below). Under these assumptions the capacitance of N such radial electrode segments would be:

$$C = N\epsilon_0 \frac{S}{d} = N\epsilon_0 \frac{Ll}{d} \eta, \quad (1)$$

where $L = R - r$ is the radial length of the electrode, $l = (R + r)/2$ is the position of its centre from the axis of rotation and η is the angle of overlap between any two opposite segments and S is the surface area of overlap. Near to any of its non-overlapping resonant modes, the entire device can be treated as a damped harmonic torsional oscillator, obeying the dynamical equation

$$I\ddot{\theta} + \Gamma\dot{\theta} + k\theta = \tau_0 e^{j\omega t}, \quad (2)$$

where I is the total moment of inertia of the system (including any liquid possibly moving with the cell), θ is the angular displacement, Γ is a dissipation factor, k the torsional spring constant, and τ_0 the amplitude of the driving torque. The well-known solution corresponds to a Lorentzian resonance with a maximum angular velocity at frequency $f_0 = 1/(2\pi)\sqrt{k/I}$, a linewidth $\Delta f = \Gamma/(2\pi I)$, and an amplitude of angular velocity $\Omega_0 \equiv \max(|\dot{\theta}|)$ given by $\Omega_0 = \tau_0/\Gamma$. Thus the expected angular velocity at resonance may be expressed from the driving torque and the linewidth as

$$\Omega_0 = \frac{\tau_0}{2\pi I \Delta f}. \quad (3)$$

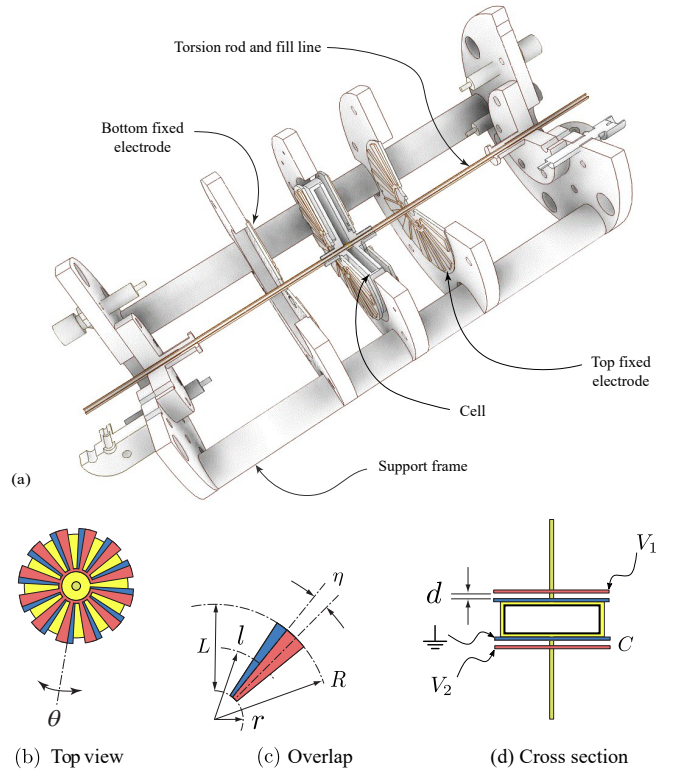


FIG. 2. (a) Drawing of the assembly, showing the torsional oscillator with circular electrodes and its surrounding frame. The pill-box-shaped helium cell is in the centre, and the fixed electrodes have been pulled away from it for clarity though, in reality, they are positioned very close to it as shown in (d). (b) Top view of the oscillator. The moving electrodes are shown in blue and the fixed electrodes in red. (c) Detail of the electrode overlap geometry. The angle η is the overlap angle between each pair of facing electrodes. (d) Profile view of the oscillator showing the torsion rod and the gaps between the capacitor plates. The drive voltage V_1 includes both the DC bias and the AC drive signal, while the detection electrode voltage V_2 stays at the level of the DC bias at all times, necessitating a DC-insulated low impedance amplifier for the detection current.

Consequently, the often-used “height-times-width-overdrive” (HW/D) parameter $\Omega_0 \Delta f / \tau_0$ then depends only on the total moment of inertia and is unaffected by changes in damping. In contrast to the conventional geometry, the narrow gap between the electrodes remains fixed, and the changes of capacitance arise on account of variations of the overlap angle during oscillation. With 12 electrodes, $R = 20$ mm, $r = 7.5$ mm giving $L = 12.5$ mm and $l = 13.75$ mm with a gap of $100\ \mu\text{m}$ and an overlap of 6° , we expect a capacitance of 19.1 pF.

For a potential difference V , the electric energy stored in the capacitor is

$$U = \frac{1}{2} CV^2 = \frac{1}{2} \epsilon_0 \frac{NLI}{d} \eta V^2. \quad (4)$$

Using the principle of virtual work with the angular displacement given by a variation of η , at constant voltage, the torque

being applied to the oscillator can be computed as³¹

$$\tau = \frac{1}{2} \epsilon_0 \frac{NLL}{d} V^2 = \frac{1}{2} \frac{C}{\eta} V^2, \quad (5)$$

where the value of the constant C/η depends only on geometry. The value of C can easily be measured at equilibrium where the value of η is fixed at 6 degrees by construction. The torque always tends to increase the overlap between the capacitor plates and does not depend on the sign of the potential V . In reaction to a fixed angular displacement θ , the BeCu torsion rod exerts an opposite torque leading to an equilibrium angular displacement which in practice is of the order of tens of micro-degrees. The driving torque, parabolic in V , can be linearised by using a large DC bias voltage V_{DC} together with a lower AC drive V_{AC} , leading to the torque

$$\tau = \frac{\xi_1 C_1}{\eta} V_{DC} V_{AC}, \quad (6)$$

where C_1 is the capacitance of the drive electrode, and ξ_1 is an efficiency factor, less than unity, that encapsulates the non-ideal behaviour of the drive of the real system. Conversely, assuming a fixed DC bias voltage on the detection electrode, we get the detection current

$$i_{det} = \dot{q} = \dot{C}_2 V_{DC} = \frac{\xi_2 C_2}{\eta} V_{DC} \Omega, \quad (7)$$

where q is the charge stored in the detection capacitor of capacitance C_2 and ξ_2 is a detection efficiency factor of less than unity. We can then express the oscillator angular velocity Ω in terms of a voltage output u from an I/V converter (transimpedance amplifier) with gain G

$$\Omega = \frac{\eta}{\xi_2 C_2 V_{DC}} \frac{u}{G}. \quad (8)$$

All quantities are known or can be measured accurately, except for the efficiency factors ξ_1 , ξ_2 and $\eta \approx 6^\circ$. The error in the overlap angle can be estimated. We are using centering pins of diameter 0.5 mm at a radius of 20 mm for fixing the electrodes. An overestimation of half a pin diameter gives an uncertainty of 0.72° , i.e., 12%. Therefore, within the idealized treatment with $\xi_1 = \xi_2 = 1$, one might expect to calculate the velocity from the measured signal to within 12%.

For practical purposes we also define the electrical equivalent HW/D parameter of the resonator, p_{HWD} , (c.f. below Eq. (3)), as

$$p_{\text{HWD}} \equiv u \frac{\Delta f}{V_{AC}} = \frac{1}{2\pi I} \frac{\xi_1 \xi_2 C_1 C_2 G V_{DC}^2}{\eta^2}. \quad (9)$$

Because in reality the oscillator is far from ideal, we found it necessary to calibrate it against direct velocity measurements, performed optically with a laser vibrometer at room temperature. We found that the velocity calculated from the electrical signal was substantially lower than that from the optical measurements, i.e. that $\xi_1, \xi_2 < 1$.

Before discussing the calibration procedure, there is one other observation that we should mention. In testing the oscillator at room temperature, we found that the copper covered

conventional fibreglass PCB material known as FR4 circuit board³² forming the substrate of the electrodes is not electrically inert: Over a few hours, the material gradually charges towards the voltage applied to the electrode, thereby destroying the designed geometry and potentials, and consequently reducing the signal obtained. It seems plausible that humidity (water content in the porous plastic) could be responsible for the residual conduction and, indeed, both surface and volume conduction are known properties of FR4 boards. At liquid nitrogen temperature (77 K), however, the problem did not arise, or developed so slowly as to be undetectable over the duration of an experiment. Subsequently, therefore, we ensured that the cell remained at zero voltage (grounded) to minimize spurious effects due to polarization of the FR4 for at least a day before cooling, or prior to making quick measurements at room temperature.

Further analyses have been carried out using three separate oscillators, to measure and then compare the velocity calculated from the lock-in amplifier signal with the optically-measured velocity. First we used a conventional oscillator as shown in Fig. 1, as a standard for the measurement setup: having previously measured identical results for this particular oscillator from two entirely different setups, we felt confident in using it as a consistency check for our instrumentation. With the conventional oscillator there is an almost 1:1 correspondence between the optically-measured angular velocity and the angular velocity calculated from the lock-in signal, as seen in Fig. 3(a).

For the present oscillator, it is clearly essential to establish a calibration procedure to determine the real torques and angular velocities from the lock-in measurements, i.e. to evaluate the two efficiency factors ξ_1 and ξ_2 . Given that data from consecutive measurements in cryogenic vacuum are highly reproducible (see Fig. 4 below), it is clear that the FR4 conduction effect is absent at low temperatures. It is therefore preferable to calibrate the oscillator under cryogenic conditions. This can be achieved similarly to the approach used earlier for quartz tuning forks³³, provided that the driving power, P , is known. In terms of electrical quantities, the AC driving power (averaged over one period) is $P = V_{AC} i_{AC} \cos \phi$, where the voltage and current are expressed as rms values and ϕ is the phase shift between the current and voltage, approaching $\pi/4$ for the capacitive drive. The same power can be expressed in terms of mechanical quantities $P = \tau_0 \Omega_0 / 2$, where τ_0 and Ω_0 represent the amplitudes of the torque and angular velocity at resonance, respectively. Both the driving current and the phase factor at resonance can be measured directly. From the measured ratio of the drive voltage to the detection current (effectively the electro-mechanical impedance Z of the device), $Z = V_{AC} / i_{det} = \tau_0 / \Omega_0$. Thus we arrive at the calibration relations

$$\Omega_0 = \sqrt{2P/Z}, \quad (10)$$

$$\tau_0 = \sqrt{2PZ}, \quad (11)$$

which can be used to determine the efficiency factors in Equations (6) and (7) by providing an indirect electrical measurement of the angular velocity Ω_0 and the torque τ_0 , while all other quantities are known or can be measured directly. We

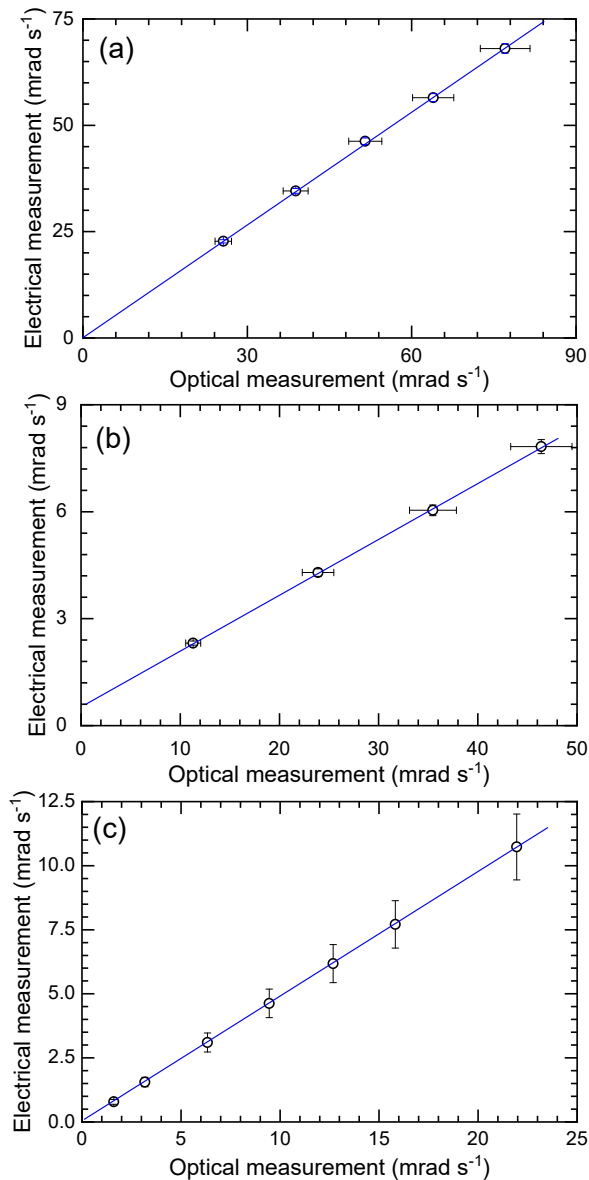


FIG. 3. Comparisons of angular velocities obtained in different ways at room temperature, for the three oscillators discussed in the text. In each case, the ordinate plots the actual velocity as measured optically, and the abscissa plots the velocity as calculated from the lock-in signal. (a) Conventional oscillator. A line fitted to the data has a slope of 0.88. (b) Torsional oscillator of the design shown in Fig. 2 with circular electrodes made of FR4. A fitted line has a slope of 0.16 and does not pass through the origin. (c) Torsional oscillator of the design shown in Fig. 2 but with all-metal electrodes and no FR4. The fitted line has a slope of 0.49.

may also note that if the driving current measurement is unavailable, so that a full calibration in the sense described above is impossible, one may still obtain the product of the two efficiency factors from Eq. (9), requiring only the knowledge of the total moment of inertia, I .

In testing the present torsional oscillator we were careful to minimise any effects from the FR4 conduction (see above). It

can be seen from Fig. 3(b) that the slope of the fitted line does not pass through zero; the value of the slope is 0.16. Despite minimising the measurement time, the conduction and charging of the FR4 must inevitably have introduced errors in measurements made at room temperature, which may be another reason why the slope does not pass through zero. Our final test used an oscillator with all-metal electrodes made of brass of thickness 1.5 mm, without any FR4 at all. As can be seen in (c) the slope is 0.49, which is markedly more than the 0.16 obtained from the FR4 oscillator. The slopes of the curves give values of the detection efficiency factor ξ_2 . There is still a discrepancy in the actual velocity. We are currently unsure of the reason, but it could be due in part to edge effects: decreasing the capacitor gap of the detection electrode, and therefore increasing the overall capacitance, further increased ξ_2 i.e. the discrepancy between the optical and electrical velocities decreased.

During the development of the torsional oscillator we investigated the effects of different diameter torsion rods, made from both BeCu and Sterling silver. The Sterling silver rods yielded a lower maximum oscillator velocity than we expected, produced characteristics that became non-linear at about 9 mm s^{-1} , and cracked the cell on thermal cycling. We therefore concentrated our designs on cells with BeCu torsion rods. We now present test data from two oscillators with BeCu torsion rods. Each of them was installed in a dilution refrigerator, with the fill line and the copper framework (Fig. 2) thermally anchored to the mixing chamber at $\sim 15 \text{ mK}$.

The first oscillator had a BeCu torsion rod of 1.2 mm OD and 0.9 mm ID. The capacitor plates were set as close as possible while avoiding touches; the resultant capacitances of the drive and detection electrode pairs were measured as 11.1 pF and 11.3 pF respectively. Our measurements yielded an efficiency factor $\xi_2 = 1/2.78$. The device worked well with a resonance frequency 79.105728 Hz, quality factor $Q \simeq 37,800$, as illustrated in Fig. 4(a).

The second oscillator had a larger diameter (stiffer) BeCu torsion rod of 1.6 mm OD and 1.24 mm ID and. The resultant capacitances were 11.93 pF and 12.04 pF for the drive and detection electrodes, respectively. It had a resonance frequency 123.18590 Hz, and a quality factor $Q \simeq 34,250$, as illustrated in Fig. 4(b). This oscillator had an efficiency factor $\xi_2 = 1/2.63$.

The mechanical Q 's of both oscillators are relatively low compared with the conventional design which can have Q 's of between 10^5 and 10^7 depending on the material used and any heat treatment for the torsion rod: apart from the lack of heat treatment of our rods, another possibly relevant factor is that the present oscillator is rigidly connected to a polymer experimental cell, and such materials are inherently lossy.

In each case, repeating the frequency sweeps over an interval of several hours showed that the data were highly reproducible, as shown in the corresponding figures. Testing the stability of the 79 Hz oscillator over 20 hours showed that the frequency was stable to within 0.03 mHz and that the 123 Hz oscillator was stable within 0.1 mHz over 10 hours. There was some vibrational noise coming from fridge pumping lines which has now been reduced by putting pumping lines in sand

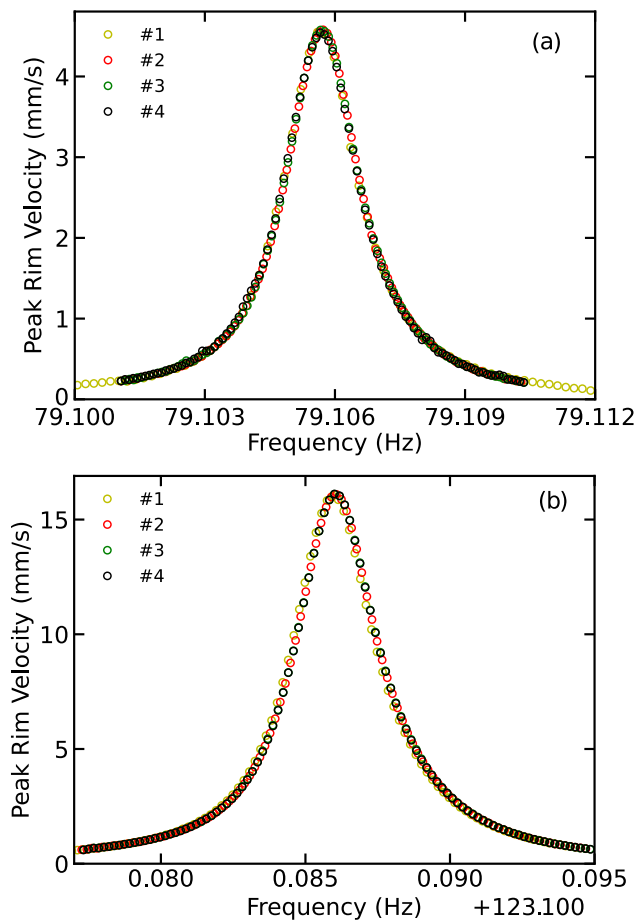


FIG. 4. Frequency sweeps in vacuum at base temperature ~ 15 mK. Four consecutive sweeps of length 10^4 s were taken over 14 hours. (a) Results from the oscillator with a 1.2 mm BeCu torsion rod, with DC bias of 200 V and an AC drive of 2.0 V. (b) Results from the 1.6 mm BeCu torsion rod oscillator, with DC bias of 600 V and an AC drive of 10.0 V.

boxes. We will test the stability of our next redesigned oscillator when installed in the dilution unit. Conventional oscillators can have a frequency stability of $1 \mu\text{Hz}$ down to several nano Hz in high Q oscillators.

At higher velocities, both oscillators exhibited Duffing-style non-linearities with asymmetry in the resonance curves and increases in linewidth that reduced the maximum attainable velocity. This effect was smaller for the second oscillator with the stiffer, larger diameter, BeCu torsion rod. A noticeable warming of the cell was observed at the higher drives with increases of temperature from ~ 15 mK up to ~ 110 mK for the larger diameter torsion rod; and up to ~ 80 mK for the smaller one.

Amplitude sweeps in vacuum at temperature ~ 100 mK for the second oscillator (1.6 mm diameter) yielded the results shown in Fig. 5(a). Here we have plotted peak rim velocity as a function of torque on a log-log scale. The frequency fell by 7.41 mHz from 123.32145 Hz for data at ~ 100 mK and for the amplitude sweep in vacuum at 4.2 K the frequency fell

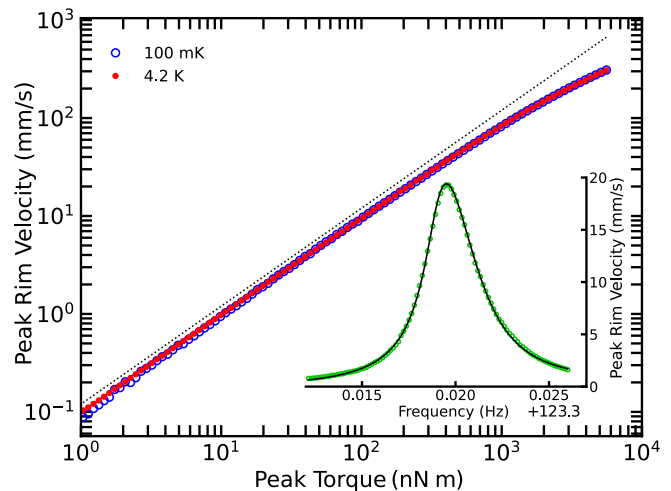


FIG. 5. Peak rim velocity dependence on peak torque with a DC bias of 800 V for the 1.6 mm BeCu torsion rod oscillator. Blue empty and red-filled circles represent vacuum data at temperatures of ~ 100 mK and ~ 4.2 K, respectively. At higher velocities shallower gradient compared to the linear dependence (dotted line) indicates an increase of damping. Inset: A frequency sweep at temperature ~ 15 mK with a DC bias of 800 V and an AC drive of 1.0 V. Slight asymmetry in the data can be described by fitting a Duffing lineshape (black line).

by 4.18 mHz from 123.31777 Hz. In each case, the resonance frequency did not fully recover its original value due to increase of fridge temperature.

We conclude that the ability of our oscillator to attain velocities of at least 300 mm s^{-1} at frequencies ~ 100 Hz means that it is well suited to studies of the generation of QT from remanent quantised vortices in superfluid ^4He , where critical velocities of this order or less are to be anticipated. The decrease in sensitivity from the change in geometry, compared to traditional cryogenic oscillators, is easily compensated by the much larger velocities that can be attained. A procedure for implementing a full calibration of the device has been established. Another immediate application could be to study a 2D spatially-modulated superfluid, where the critical behaviour expected by Choi et al¹⁶ was apparently absent up to velocities of 33 mm s^{-1} : our device would facilitate measurements at much higher velocities, and might enable a determination of the critical velocity for this state and help to elucidate its spectrum of excitations.

We gratefully acknowledge help, advice, and valuable discussions with Oleg Kolosov in relation to the optical measurements that gave us an independent method of measuring the velocity at the rim of our cell. This work was supported by the Engineering and Physical Sciences Research Council, United Kingdom [grant numbers EP/P022197/1, EP/P024203/1 and EP/X004597/1], as well as EU H2020 European 7 Microkelvin Platform (Grant Agreement 824109). DS acknowledges support from the Czech Science Foundation under Project No. 20-13001Y.

AUTHOR DECLARATIONS

Conflict of interest

The authors have no conflicts to disclose.

Author Contributions

Anthony M. Guénault: Software (lead); Investigation (supporting); Writing – original draft (equal). **Peter V. E. McClintock:** Funding acquisition (lead); Project administration (lead); Investigation (supporting); Writing – original draft (equal); Writing – review & editing (equal). **Malcolm Poole:** Funding acquisition (equal); Methodology (equal); Investigation (lead); Writing – original draft (equal); Writing – review & editing (equal). **Roch Schanen:** Conceptualization (lead); Methodology (equal); Investigation (equal); Writing – original draft (equal); Writing – review & editing (equal). **Viktor Tsepelin:** Project administration (supporting); Investigation (supporting); Writing – review & editing (equal). **Dmitry E. Zmeev:** Funding acquisition (equal); Investigation (supporting); Writing – review & editing (equal). **David Schmoranzer:** Writing – original draft (equal); Writing – review & editing (equal). **William F. Vinen:** Conceptualization (equal); Funding acquisition (equal). **Deepak Garg:** Investigation (supporting); Writing – review & editing (equal). **Kalpna Devi:** Investigation (supporting); Writing – review & editing (equal).

DATA AVAILABILITY

The data that support the findings of this study will be openly available in the Lancaster University Publications and Research (Pure) system at <https://doi.org/10.17635/lancaster/researchdata/594>.

REFERENCES

- 1 E. Andronikashvili, “A direct observation of two kinds of motion in liquid Helium II,” in *Helium 4* (translation of *J. Phys. (U.S.S.R.)* **10**, 201; 1946), edited by Z. M. Galasiewicz (Pergamon, Oxford, 1971) pp. 154–165.
- 2 A. Golov, J. V. Porto, K. Matsumoto, L. Pollack, E. N. Smith, R. D. Biggar, T. L. Ho, and J. M. Parpia, “Superfluidity of pure ^3He and mixtures of ^3He and ^4He in Aerogel,” *J. Low Temp. Phys.* **110**, 515–523 (1998).
- 3 N. Zhelev, T. S. Abhilash, E. N. Smith, R. G. Bennett, X. Rojas, L. Levitin, J. Saunders, and J. M. Parpia, “The A-B transition in superfluid helium-3 under confinement in a thin slab geometry,” *Nat. Comm.* **8**, 15963 (2017).
- 4 J. Nyèki, A. Phillis, A. Ho, D. Lee, P. Coleman, J. Parpia, B. Cowan, and J. Saunders, “Intertwined superfluid and density wave order in two-dimensional ^4He ,” *Nat. Phys.* **13**, 455–459 (2017).
- 5 J. E. Berthold, D. J. Bishop, and J. D. Reppy, “Superfluid transition of ^4He films adsorbed on porous Vycor glass,” *Phys. Rev. Lett.* **39**, 348–352 (1977).
- 6 V. E. Syvokon, K. Ooyama, M. Fukuda, T. Obata, T. Igarashi, and M. Kubota, “Superfluid helium films in porous glass: torsional oscillator study at high AC velocities,” *Physica B* **284–288**, 113–114 (2000).
- 7 J. V. Porto and J. M. Parpia, “Superfluid ^3He in Aerogel,” *Phys. Rev. Lett.* **74**, 4667–4670 (1995).
- 8 J. Taniguchi, H. Ichida, Y. Aoki, S. Fukazawa, M. Hieda, and M. Suzuki, “Comparison between torsional oscillator and ultrasonic measurements of ^4He confined in nano-porous media,” *J. Low Temp. Phys.* **148**, 791–795 (2007).
- 9 D. J. Bishop, M. A. Paalanen, and J. D. Reppy, “Search for superfluidity in HCP ^4He ,” *Phys. Rev. B* **24**, 2844–2845 (1981).
- 10 E. Kim and M. H. W. Chan, “Probable observation of a supersolid helium phase,” *Nature* **427**, 225–227 (2004).
- 11 E. Kim and M. H. W. Chan, “Observation of superflow in solid helium,” *Science* **305**, 1941–1944 (2004).
- 12 Y. Aoki, J. C. Graves, and H. Kojima, “Oscillation frequency dependence of nonclassical rotation inertia of solid ^4He ,” *Phys. Rev. Lett.* **99**, 015301 (2007).
- 13 G. Nichols, M. Poole, J. Nyèki, J. Saunders, and B. Cowan, “Frequency dependence of the supersolid signature in polycrystalline ^4He ,” arXiv:1311.3110v2 [cond-mat.other] (2014).
- 14 A. S. C. Rittner and J. D. Reppy, “Observation of classical rotational inertia and nonclassical supersolid signals in solid ^4He below 250 mk,” *Phys. Rev. Lett.* **97**, 165301 (2006).
- 15 H. Choi, D. Takahashi, K. Kono, and E. Kim, “Evidence of supersolidity in rotating solid helium,” *Science* **330**, 1512–1514 (2010).
- 16 J. Choi, A. A. Zadorozhko, J. Choi, and E. Kim, “Spatially modulated superfluid state in two-dimensional ^4He films,” *Phys. Rev. Lett.* **127**, 26–28 (2021).
- 17 E. J. Pratt, B. Hunt, V. Gadagkar, M. Yamashita, M. J. Graf, A. V. Balatsky, and J. C. Davis, “Interplay of rotational, relaxational, and shear dynamics in solid ^4He ,” *Science* **332**, 821–824 (2011).
- 18 G. P. Bewley, D. P. Lathrop, and K. R. Sreenivasan, “Superfluid helium – visualization of quantized vortices,” *Nature* **441**, 588 (2006).
- 19 A. Eyal, X. Mi, A. V. Talanov, and J. D. Reppy, “Search for supersolidity in solid ^4He using multiple-mode torsional oscillators,” *Proc. Nat. Acad. Sci. USA* **113**, E3203–E3212 (2016).
- 20 L. Skrbek, D. Schmoranzer, Š. Midlik, and K. R. Sreenivasan, “Phenomenology of quantum turbulence in superfluid helium,” *Proc. Nat. Acad. Sci. (USA)* **118**, e2018406118 (2021).
- 21 D. D. Awschalom and K. W. Schwarz, “Observation of a remanent vortex-line density in superfluid helium,” *Phys. Rev. Lett.* **52**, 49–52 (1984).
- 22 I. M. Khalatnikov, *An Introduction to the Theory of Superfluidity* (Benjamin, New York, 1965).
- 23 E. B. Sonin, *Dynamics of Quantised Vortices in Superfluids* (CUP, Cambridge, 2016).
- 24 M. Sýkora, M. Pavelka, M. La Mantia, D. Jou, and M. Grmela, “On the relations between large-scale models of superfluid helium-4,” *Phys. Fluids* **33**, 127124 (2021).
- 25 S. K. Nemirovskii, “Comment on On the relations between large-scale models of superfluid helium-4Å” [*Phys. Fluids* 33, 127124 (2021)],” *Phys. Fluids* **34**, 069101 (2022).
- 26 M. Sýkora, M. Pavelka, M. La Mantia, D. Jou, and M. Grmela, “Response to Comment on On the relations between large-scale models of superfluid helium-4 [Phys. Fluids 34, 069101 (2022)],” *Phys. Fluids* **34**, 069102 (2022).
- 27 L. Skrbek and K. R. Sreenivasan, “Developed quantum turbulence and its decay,” *Phys. Fluids* **24**, 011301 (2012).
- 28 S. V. Talalov, “Closed vortex filament in a cylindrical domain: Circulation quantization,” *Phys. Fluids* **34**, 041702 (2022).
- 29 R. Hänninen and W. Schoepe, “Universal onset of quantum turbulence in oscillating flows and crossover to steady flows,” *J. Low Temp. Phys.* **158**, 410–414 (2010).
- 30 R. C. Richardson and E. N. Smith, *Experimental Techniques in Condensed Matter Physics at Low Temperatures* (Advanced Book Classics, Cornell, 1988).
- 31 R. P. Feynman, *The Feynman Lectures on Physics* vol. II, (Addison Wesley Longman, 1970) pp. 8–2.
- 32 Tracks Laser & Electronics, “FR4 1.6mm copper board to IPC-4101b/21 specification,” Technical specification sheet from Track Laser & Electronics Ltd, Popes Manor, Murrell Hill Lane, Bracknell, Berkshire RG42 4DA, UK (2022).
- 33 R. Blaauwgeers, M. Blazkova, M. Clovecko, V. B. Eltsov, R. de Graaf, J. Hosio, M. Krusius, D. Schmoranzer, W. Schoepe, L. Skrbek, P. Skyba, R. E. Solntsev, and D. E. Zmeev, “Quartz tuning fork: Thermometer, pressure- and viscometer for helium liquids,” *J. Low Temp. Phys.* **146**, 537–562 (2007).